Small Satellite Formation Flying Simulation with Multi-Constellation GNSS and Applications to Future Multi-Scale Space Weather Observations

YuXiang Peng, *Virginia Tech, Blacksburg, VA, USA*
Wayne A. Scales, *Virginia Tech, Blacksburg, VA, USA*
Michael C. Esswein, *Virginia Tech, Blacksburg, VA, USA*
Michael D. Hartinger, *Virginia Tech, Blacksburg, VA, USA; Space Science Institute, Boulder, CO, USA*

BIOGRAPHIES

YuXiang Peng is a Ph.D. candidate in the Bradley Department of Electrical and Computer Engineering at Virginia Tech. He received his M.S. (2017) in Electrical Engineering from Virginia Tech, and B.S. (2014) in Physics from Sun Yat-sen University. He is a graduate research assistant with the Virginia Tech Center for Space Science and Engineering Research.

Wayne A. Scales is a J. Byron Maupin Professor of Engineering in the Bradley Department of Electrical and Computer Engineering, affiliate Professor in the Crofton Department of Aerospace and Ocean Engineering, and founding Director of the Center for Space Science and Engineering Research at Virginia Tech. He received his B.S. and M.S. in Electrical Engineering from Virginia Tech, M.S. in Applied Math from Virginia Tech, and Ph.D. in Electrical Engineering and Applied Physics from Cornell University.

Michael C. Esswein is a Ph.D. student in the Crofton Department of Aerospace and Ocean Engineering at Virginia Tech. He holds a B.S. in Aerospace Engineering from the University at Buffalo.

Michael D. Hartinger is a Research Assistant Professor in the Bradley Department of Electrical and Computer Engineering at Virginia Tech and a Research Scientist at the Space Science Institute. He received his Bachelor's in Physics from Cornell University in 2006, and PhD in Geophysics and Space Physics from UCLA in 2012. Michael studies solar-wind-magnetosphere-ionosphere coupling, and he currently co-manages an array of autonomous instruments in Antarctica.

ABSTRACT

Various scales of upper atmospheric structures and their coupling mechanisms are not fully understood due to a lack of robust observation. Satellite formation flight enables identification of temporal and spatial variation of multi-scale space weather phenomena. GNSS-based small satellite formation flying enables new applications for future low-cost, versatile, geo-space observations. The Virginia Tech Formation Flying Testbed (VTFFTB), a GPS-based hardware-in-the-loop (HIL) simulation testbed for dual-satellite formation flying, was recently developed to design new ionospheric remote sensing techniques. A simple ESF scenario was simulated on the VTFFTB to demonstrate a new ionospheric measurement technique by GPS-based LEO formation flying. The objectives of this current work are to develop a newer version of VTFFTB to (i) incorporate the Galileo (E1, E5a, E5b) constellation in simulations; (ii) implement natural relative orbits for better fuel efficiency and optimal remote sensing capability, and (iii) simulate scenarios of 3-spacecraft formation flying with applications to multi-scale space weather problems.

Multi-constellation GNSS improves the relative navigation performance as well as ionospheric observation capability. Total Electron Content (TEC) and ionospheric scintillation measurements from multiple frequency bands can be sampled by a fleet of LEO satellites in proximity with respect to the GPS and Galileo constellations. HIL simulations with the additional Galileo constellation show the electron density retrieval accuracy is enhanced compared to GPS-only scenarios. Two configurations of elliptic orbits are implemented to measure electron density and thus obtain different characteristics between different GNSS constellations. A polar, sun-synchronous, elliptic orbit was chosen to simulate and validate 3-satellite real-time formation flying scenarios. A decentralized formation scheme is selected as the archetypal approach of orbit estimation and control for the multiple satellite group. Three different formation configurations (leader-follower → elliptic-orbit → side-by-side) are considered in order to test the maneuverability of a

 https://doi.org/10.33012/2019.16883

multi-scale observation campaign in response to real-time geomagnetic conditions. A number of space weather phenomena can be observed by applying this new observation technique of using scalable small satellite formation clusters. The VTFFTB will ultimately become a mission incubator for future multi-scale geo-space environment observing systems using GNSS-based small satellite formation flying.

INTRODUCTION

Space weather monitoring is important in order to predict or prevent potential hazards for modern technology or space missions. Numerous kinds of space weather effects on satellite communication and radio navigation systems (e.g. GPS) directly affect our daily life activities. Investigating the coupling mechanisms between atmospheric gravity waves (AGW) and traveling ionospheric disturbances (TID) is beneficial for us to detect or predict natural hazards (e.g. earthquakes, tsunamis, volcanic eruptions, etc.) [1]. However, various scales of structures or phenomena and their coupling mechanisms in the ionosphere and magnetosphere are not fully understood due to a lack of robust observation. Many traditional satellite missions deployed relatively massive spacecraft with expensive scientific payloads to probe the space environment. Recently, the concept of small satellite constellation or formation flying becomes a trending technology because of various advantages over a single large satellite. Satellite formation flight is an ideal mission architecture to better identify temporal and spatial variation of multi-scale space weather phenomena. For example, spacecraft formation flight missions such as MMS (Magnetospheric Multiscale) [2] and Cluster [3] measure phenomena in the solar wind, magnetopause, magnetotail and radiation belts using scalable tetrahedral configurations that consists of four satellites. Deploying a group of small satellites or Cubesats as a team can be cheaper, more flexible, more sustainable, and even more robust so that they can outperform single satellite missions. A number of nanosatellite (mass = 1 - 10 kg) constellation missions with applications to space science and dozens of nanosatellite formation flying missions for technology demonstration are summarized in [4]. However, few small satellite formation flying missions have been developed and directly applied to space weather observations.

Because of the inhomogeneous refractive index of the Earth's ionosphere, Global Navigation Satellite System (GNSS) signals will be delayed (associated with total electron content or TEC) while penetrating through the Earth's upper atmosphere as well as refracted (associated with radio occultation or RO). When the propagating GNSS signals encounter certain scales of ionospheric irregularities (that correspond to the Fresnel size of the radio wavelength), the signal amplitude or phase could fluctuate and lead to ionospheric scintillations [5]. Because of ionospheric impact on GNSS signals, multi-frequency GNSS receivers are appropriate tools for ionosphere remote sensing. The MIT Madrigal database utilizes ground-based multi-frequency GPS data from thousands of stations around the world to generate global vertical TEC maps since 1998 [6]. Using ground-based GNSS TEC networks, the 4-D ionospheric (electron density) profile can be obtained by 3-D ionospheric tomography techniques [7]. Typically ground-based GPS networks are only able to cover the continental regions, therefore satellite-based ionospheric sounding techniques such as GNSS-RO, in-situ, or space-based tomography are implemented to fill the data gaps in the ocean regions. Following the success of the COSMIC (Constellation Observing System for Meteorology, Ionosphere, and Climate) GPS-RO mission [8], Spire Global Inc. has been launching a large CubeSat constellation into LEO to conduct GNSS-RO measurements in the ionosphere with unprecedented coverage [9]. The plasma sensors on the Defense Meteorological Satellite Program (DMSP) satellites collect in-situ measurements of plasma density [10]. Yizengaw et al. conducted space-based tomography to routinely determine ionospheric average electron density profiles using the dual-frequency GPS data on the LEO FedSat satellite [11]. Such space-based tomographic retrieval profiles describe the time-averaged behavior of the ionosphere very well, however, they are limited in resolving the temporal variation of multi-scale plasma structure.

Because of the superb performance in relative position based on the carrier-phase differential GNSS technique, GNSS is an ideal tool of relative navigation for spacecraft formation flying. Together with the promising GNSS remote sensing capability, GNSS-based satellite formation presents affordable new opportunities for multi-scale ionospheric remote sensing. The Virginia Tech Formation Flying Testbed (VTFFTB), a hardware-in-the-loop (HIL) simulation testbed for GPS-based formation flight, was developed for ionospheric remote sensing applications [12]. An equatorial spread F (ESF) scenario was simulated on the VTFFTB to demonstrate new measurement techniques for ionospheric irregularities.

The purpose of this work can be categorized into two different phases. First, the VTFFTB is upgraded into a multi-constellation (GPS + Galileo) version with enhanced capability on ionospheric sounding and relative navigation [13]. A more fuel-efficient relative orbit is implemented to probe the ionosphere in an ESF scenario. Since only one LEO GNSS receiver was incorporated during earlier work, previously the VTFFTB only simulated a pair of satellites in formation by simulating the uncontrolled chief satellite scenario first and then running the deputy satellite scenario with real time guidance navigation and control (GNC) later. Compared to dual-

satellite formation, 3-satellite formation flying further increases the temporal and spatial resolution of ionospheric measurements by forming a scalable triangle geometry. Particularly, a team of three multi-frequency GNSS receivers would enable multi-point (2 or 3) electron density (N_e) retrieval, which offers improved characterization compared to single-point N_e sounding in the previous dual-satellite scenarios. Using the relative geometry within the 3-satellite fleet, it will be easier to "track" ionospheric irregularities that cause GNSS scintillations. Therefore, the second phase of this work is to further extend the VTFFTB into a multi-satellite version using three independent satellite for real-time formation flying scenarios. A polar orbit scenario is designed to verify the formation flying fleet maneuver by HIL real-time simulations. To optimize the autonomy and maintain mission robustness during GNSS degraded environments (e.g. scintillation), the decentralized archetypal approach is chosen over the centralized principle as the formation navigation and control scheme for the new version of VTFFTB. Different formation configurations and the reconfiguration maneuvers will be simulated and presented with potential applications to a proposed space weather campaign. Candidate space weather phenomena proposed to be observed include ionospheric plasma bubbles, mid-latitude trough, HmF2/hmF2, polar cap patches, tongues of ionization and ultra-low-frequency (ULF) plasma waves. With the integrated HIL simulation capability between satellite formation flying and space weather impacts on multi-constellation GNSS signals, the VTFFTB may serve to be a versatile mission incubator for future multi-scale space weather observing systems using small satellite formation flying.

INFRASTRUCTURE OVERVIEW

Two versions of the VTFFTB for two corresponding phases of work are presented as follows.

Multi-constellation VTFFTB for 2-satellite Formation Flight

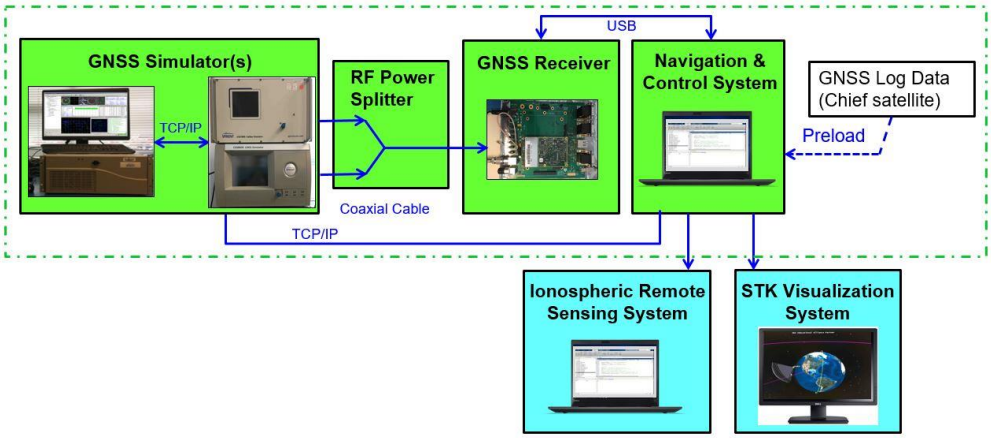

Fig. 1: System configuration of the multi-constellation VTFFTB for 2-satellite formation flight

The multi-constellation version of the VTFFTB was developed based on the previously established GPS-only version. The overall infrastructure of the multi-constellation version is shown in Fig. 1. Designed for two LEO spacecraft formation flight, this HIL simulation testbed mainly includes five different components: a GNSS simulator, a GNSS receiver, a navigation & control system, an ionospheric remote sensing system, and a STK visualization system. The GNSS simulator consists of a Spirent GSS8000 GPS (L1, L2 & L5) RF signal generator, a Spirent GSS7800 Galileo (E1, E5a, E5b & E5 AltBOC) RF signal generator, and a master computer with the simulation control software SimGEN. Ionospheric impacts on GNSS signals can be designed and simulated via customizing the TEC and amplitude scintillation (S4) profiles. The simulated GNSS signals output from the two RF generators are mixed by a RF power splitter and then fed to the GNSS receiver. The NovAtel OEM628 receiver is used to track the multi-frequency multi-constellation GNSS signals at a LEO satellite platform. Written as a MATLAB software package, the navigation & control system acquires the GNSS data from the receiver via a USB (Universal Serial Bus) interface for real-time relative orbit estimation and control. A single-differential carrier-phase measurement model is implemented with a satellite relative orbit propagtor to drive an Extended Kalman filter (EKF) and estimate the relative states between the chief and deputy satellites [14]. The current relative states (e.g. position and velocity) between the two satellites together with the desired relative states are input into a flight control subsystem, to compute the required thrust for translational control. The attitude control is ignored in the current simulations but can

be added on demand. The control algorithm employs a state-dependent Riccati equation (SDRE) technique [15] based on the Hill-Clohessy-Wiltshire (HCW) relative motion model, and the implementation is similar to the approaches in [16]. The computed thrust is applied to the deputy satellite in the next time step for formation keeping or re-acquisition maneuvers. Every time step, the satellite motion commands are generated and transferred back to the GNSS simulator via TCP/IP to propagate the satellite (with onboard GNSS receiver) trajectory. This forms a closed-loop feedback system within the green-dashed box in Fig. 1. The default rate for GNSS data logging, estimation, and control is 1 second.

The GNSS data is not only used for navigation purposes, but also applied to ionospheric measurements. Developed as a MATLAB software package, the ionospheric remote sensing system processes the GPS and Galileo data collected from the receiver, and then produces TEC and effective S4 indices between the tracked GNSS satellites and the LEO fleet. When the two LEO satellites fly at different altitudes, the vertical N_e in between can be retrieved and the results are sensitive to the noise level and altitude offset. These ionospheric products offer a good opportunity to routinely measure the N_e profile or detect ionospheric irregularities. The STK visualization system in the VTFFTB is able to visualize the spacecraft trajectory in real-time or replay mode, by transferring the motion data into the AGI's (Analytical Graphics, Inc.) physics-based simulation software Systems Tool Kit (STK).

VTFFTB for 3-satellite Formation Flight

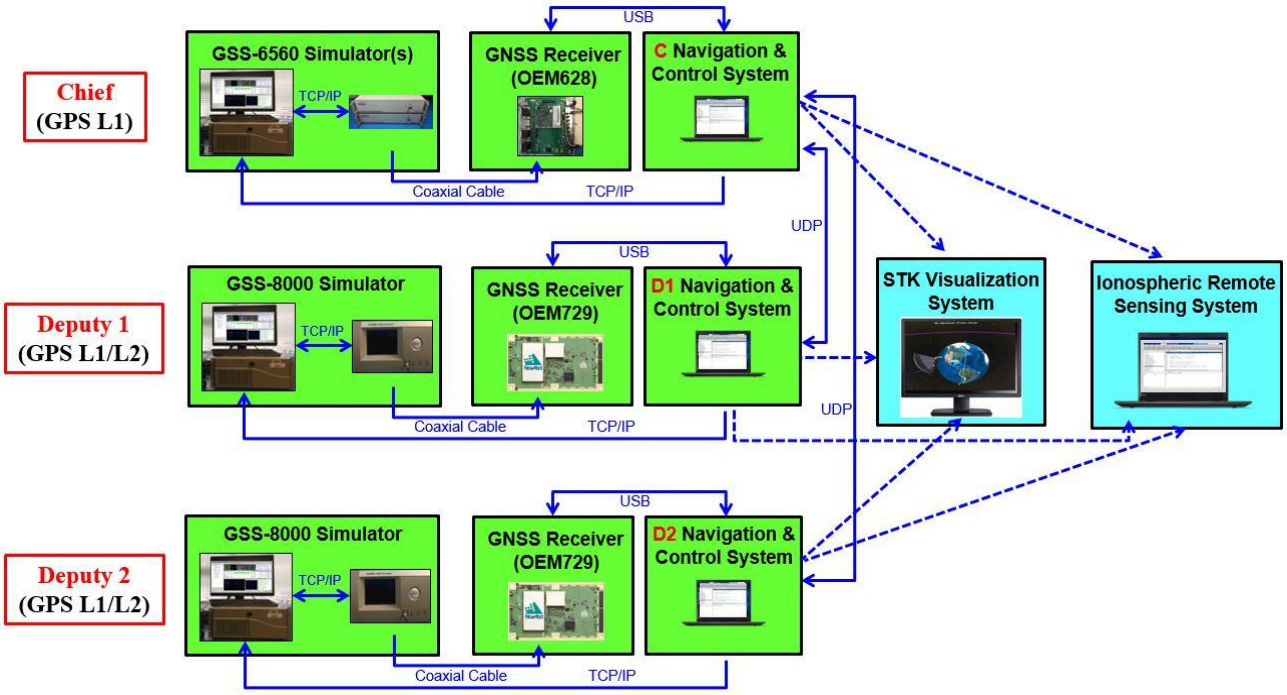

Fig. 2: System configuration of the VTFFTB for triple-satellite formation flight

The multi-satellite version of VTFFTB was established by incorporating additional GNSS simulators and receivers. The overall infrastructure is presented in Fig. 2. Three independent closed-loop satellite systems, including a chief and two deputies, communicate with each other via the User Datagram Protocol (UDP) message package. Each satellite system comprises a GPS simulator, a GNSS receiver, and a navigation & control system. Three identical Lenovo laptops are acquired to serve as on-board computers for each satellite's navigation and control system. For the uncontrolled chief satellite system, a NovAtel OEM628 receiver is utilized to track the GPS L1 signals from a Spirent GSS6560 GPS simulator. Due to the simulator's default limitation, no TEC or scintillation can be simulated for chief satellite scenarios at this time. For the controlled Deputy 1 satellite system, a NovAtel OEM729 receiver is used to track the GPS (L1, L2) signals from the Spirent GSS8000 simulator. For the controlled Deputy 2 satellite system, another NovAtel OEM729 receiver is used to track the GPS (L1, L2) signals from another Spirent GSS8000 GPS simulator. Following the protocol of decentralized formation control, each deputy satellite uses the GPS data broadcasted from the Chief via UDP plus its own GPS data for relative navigation and control. TEC and scintillation can be simulated in both deputy satellites'

scenarios. After each simulation, all GNSS data are transferred to the ionospheric remote sensing system for post-processing and the STK visualization system for scenario replay. Only the vertical N_e between the two deputy satellites can be retrieved based on this current setup, but in principle the N_e between the Chief and two deputies can be obtained as well (it is planned to replace the simulator for the Chief satellite with a dual band GPS/GNSS simulator in the near future).

SIMULATION SCENARIOS

Three HIL simulation scenarios are now described that are used to illustrate applications of the VTFFB in the following section.

Baseline Two-Satellite ESF Scenario

The ESF scenario designed and simulated in [12] is used as the baseline scenario for multi-constellation GNSS HIL formation flying simulation on the VTFFTB in Fig. 1. A brief review of the scenario is given here. As a type of ionospheric irregularity that appears in the equatorial region after sunset, ESF often reveals itself as ionospheric plasma bubbles or plumes (unstable regions of electron density depletion) generated by plasma instabilities. Plasma bubbles can cause extra signal delay (or TEC gradients) and scintillation on GNSS signals. Therefore, the GNSS receivers can be a sensor for ESF monitoring or observations as well [5].

In SimGEN, simplified ionospheric impacts on GNSS signals can be emulated by the customizing the TEC and/or S4 profile. The built-in TEC modelling capability features the Klobuchar model, the NeQuick model, or a spacecraft TEC profile that takes into account the ionization level at different altitudes in the ionosphere. The spacecraft TEC profile feature is adopted to model plasma bubbles. By default, however, there is no horizontal or temporal variation of electron density in such plasma bubble simulations. On the other hand, amplitude scintillation can be simulated by modelling the S4 index in a horizontal grid with a minimum resolution of 10° latitudinally by 15° longitudinally. Also the scintillation events are confined under an altitude limit of 350 km. Given these simulation capabilities, a cuboid region of plasma bubbles was modelled by setting up the S4 profile and spacecraft TEC profile. To represent the scintillation effects on GNSS signals caused by ESF, the S4 value is applied as 0.4 in the region between 290 km and 350 km vertically, 0° to 10° South latitudinally, and 20:00 to 21:00 local time (LT) longitudinally. This region is right above the Jicamarca Radio Observatory (JRO) in Peru where plasma bubbles and scintillations are routinely observed [17]. A vertical N_e profile measured by the PLUMEX I sounding rocket (SR) campaign [18] is used to derive the vertical TEC profile in this ESF scenario with 3 plasma bubbles at different altitudes.

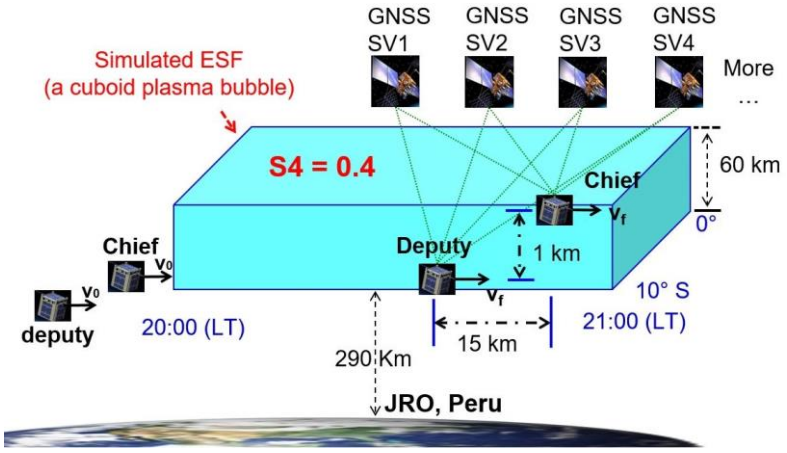

Fig. 3: Illustration of the ESF scenario [13]

In this scenario; an elliptical, low-inclination, LEO orbit is chosen for the satellite fleet to probe different ionospheric layers and monitor the equatorial region. As for a baseline relative orbit illustrated in Fig. 3, a 15-km in-track offset and a 1-km radial offset are chosen as the default formation keeping mode while measuring the plasma bubbles. Considering the default 1-second logging rate and a nominal LEO satellite horizontal velocity of 7 or 8 km/s, a 15-km separation is enough to allow the two LEO GNSS receivers sense different characteristics while penetrating a boundary of ionospheric irregularities. Since the two LEO satellites are located at

different altitudes, the vertical N_e between the two GNSS receivers can be approximately computed by differencing the vertical TEC and then dividing the vertical separation (~ 1 km in this case).

Two-satellite ESF Scenario using Natural Orbits

Maintaining a constant radial offset is not a fuel-efficient formation configuration. Hence, natural relative orbits are also considered in this work to make observations in the ESF scenario. Natural orbits are bounded relative motion following specific initial conditions under the HCW relative motion model and are extremely fuel efficient even upon adding perturbations. To analyze the relative dynamics of spacecraft formation flying, the body frame is established to describe relative states that originate from the center of mass of a spacecraft (the chief in this context). As shown in Fig. 4, the unit vector $\hat{e}_x$ denotes the radial direction (from the center of the Earth to the chief satellite). The unit vector $\hat{e}_y$ denotes the "in-track" or "along-track" direction (aligned with the velocity vector of the chief satellite). The unit vector $\hat{e}_z$ denotes the "cross-track" direction with the positive direction following with the angular momentum vector. In the body frame, the relative position can be expressed as: $\rho(t) = \delta r(t)\ \hat{\mathrm{e}}_x + r_c\delta\theta(t)\ \hat{\mathrm{e}}_y + \delta z(t)\ \hat{\mathrm{e}}_z$, where r_c is the orbital radius of the chief satellite. The initial relative position is defined as: $\rho(0) = \delta r_0\ \hat{\mathrm{e}}_x + r_c\delta\theta_0\ \hat{\mathrm{e}}_y + \delta z_0\ \hat{\mathrm{e}}_z$ and the initial relative velocity is defined as: $\dot{\rho}(0) = \delta\dot{r}_0\ \hat{\mathrm{e}}_x + r_c\delta\dot{\theta}_0\ \hat{\mathrm{e}}_y + \delta\dot{z}_0\ \hat{\mathrm{e}}_z$.

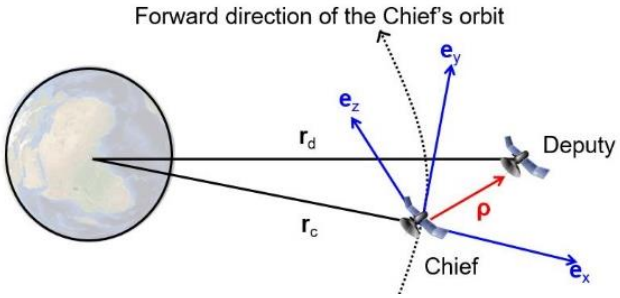

Fig. 4: Body-frame of satellite formation flying

Given the bounding condition of $r_c\delta\dot{\theta}_0 = -2n\delta r_0$ (where the mean motion $n = \sqrt{\frac{\mu}{r_c^3}}$), the relative position in each body-frame direction would become [19]:

$$\delta r(t) = \delta r_0 \cos(nt) + \frac{\delta\dot{r}_0}{n}\sin(nt) \quad \textbf{(1)}$$

$$r_c\delta\theta(t) = r_c\delta\theta_0 - 2\delta r_0 \sin(nt) + \frac{2\delta\dot{r}_0}{n}\cos(nt) - \frac{2\delta\dot{r}_0}{n} \quad \textbf{(2)}$$

$$\delta z(t) = \delta z_0 \cos(nt) + \frac{\delta\dot{z}_0}{n}\sin(nt) \quad \textbf{(3)}$$

On the other hand, the relative velocity in each direction would become:

$$\delta\dot{r}(t) = -n\delta r_0 \sin(nt) + \delta\dot{r}_0 \cos(nt) \quad \textbf{(4)}$$

$$r_0\delta\dot{\theta}(t) = -2n\delta r_0 \cos(nt) - 2\delta\dot{r}_0\sin(nt) \quad \textbf{(5)}$$

$$\delta\dot{z}(t) = -n\delta z_0 \sin(nt) + \delta\dot{z}_0 \cos(nt) \quad \textbf{(6)}$$

Based on the Eq. (1) – (6), an in-plane elliptic relative orbit is designed as shown in Fig. 5. Two similar configurations are simulated with a maximum radial offset of 2000-m and 10000-m, respectively. Both formation configurations do not have any cross-track (out-of-plane) movement. During a 1-hour simulation period using the OEM729 receiver, the altitude difference between two LEO satellites changes continuously. Therefore, there are two moments where the height difference is zero (~ 0 second and ~0.8 hours).

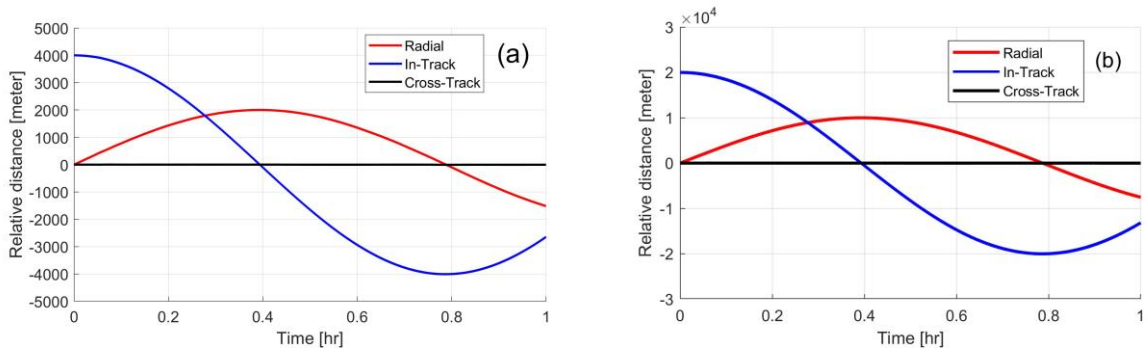

Fig. 5: in-plane elliptic relative orbit (a) 2-km maximum radial offset; (b) 10-km maximum radial offset

Three-satellite Polar Orbit Scenario using Natural Orbits

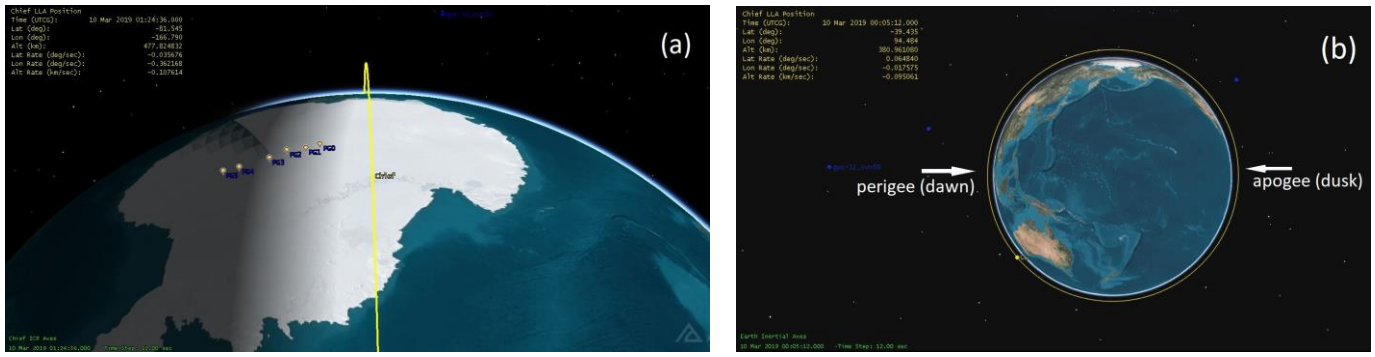

Fig. 6: Polar orbit scenario: (a) Cross-track view; (b) Along-track view

A polar orbit scenario is designed as a "quality check" for the 3-satellite real-time formation flight simulation on the VTFFTB in Fig. 2. The total simulation time is 1.5 hours. The chief satellite orbit is designed first to determine the trajectories for the entire satellite fleet. A sun-synchronous orbit is selected to get reliable solar power from the Sun, and pass Antarctica and the Arctic to simulate observing multi-scale space weather phenomena in the polar regions. Also, this enables the possibility of conducting a multi-instrument geo-space observation campaign by incorporating an existing ground-based network, such as the six AAL-PIP (autonomous adaptive low-power instrument platform [20]) stations indicated by PG0 – PG5 in Fig. 6 (a), or SuperDARN radars [21] that point toward the polar caps. The AAL-PIP measures ground-based magnetic field, GPS TEC and scintillations, while the SuperDARN radars observe plasma flows. All of these measurements are complimentary to the TEC, S4, and electron density retrieved by the LEO satellite fleet. The orbital eccentricity is taken to be non-zero so that the fleet can sense different ionospheric layers/altitudes. Particularly, the perigee is set at the dawn side equator at ~350 km, while the apogee is set at the dusk side equator at ~550 km, as denoted in Fig. 6 (b). The satellite fleet will then be able to follow the ionospheric height difference between dawn and dusk, or possibly track the height maximum of the F2 layer (or hmF2). Now that the chief trajectory is determined, the orbit between the two deputy satellites relative to the chief satellite is considered next. To optimize the fuel budget, the natural dynamics of relative motion is utilized during the formation flying including three different phases of formation configuration: (1) leader-follower in-plane formation; (2) elliptic-orbit in-plane formation; (3) side-by-side out-of-plane formation. The reacquisition switching formation geometry, can potentially be a useful maneuver during geomagnetic storms so that a specific upper atmospheric structure can be detected by the satellite fleet. This concept may also be applied to ultimately develop an active feedback LEO formation configuration for varying space weather conditions.

The software simulation module in the VTFFTB is based on a 2-body dynamic model. The relative motion using natural orbits for the two deputy satellites are designed and simulated as shown in Fig. 7. The deputy 1 (D1) satellite's relative orbit history across three different configurations are shown together with the thrust history given a maximum thrust limit (ΔV_{max}) of 0.3 m/s^2. First D1 was leading 100 meters ahead of the chief satellite for 15 minutes, and then flew up and back relative to the chief to perform an

elliptic orbit for 45 minutes, and finally entered a side by side out of plan formation mode for the last 30 minutes. Similar symmetrical relative motion was designed for the deputy 2 (D2) satellite. First the D2 followed the chief 100 meters behind, and then flew down and forward relative to the chief, and eventually returned toward the chief in a side by side formation opposite to D1. The fuel budget for both deputy satellites are symmetrical and efficient overall. Between phase 2 and 3, a small amount of fuel was spent in the along-track direction to pull the deputy satellites back to the chief as a formation acquisition.

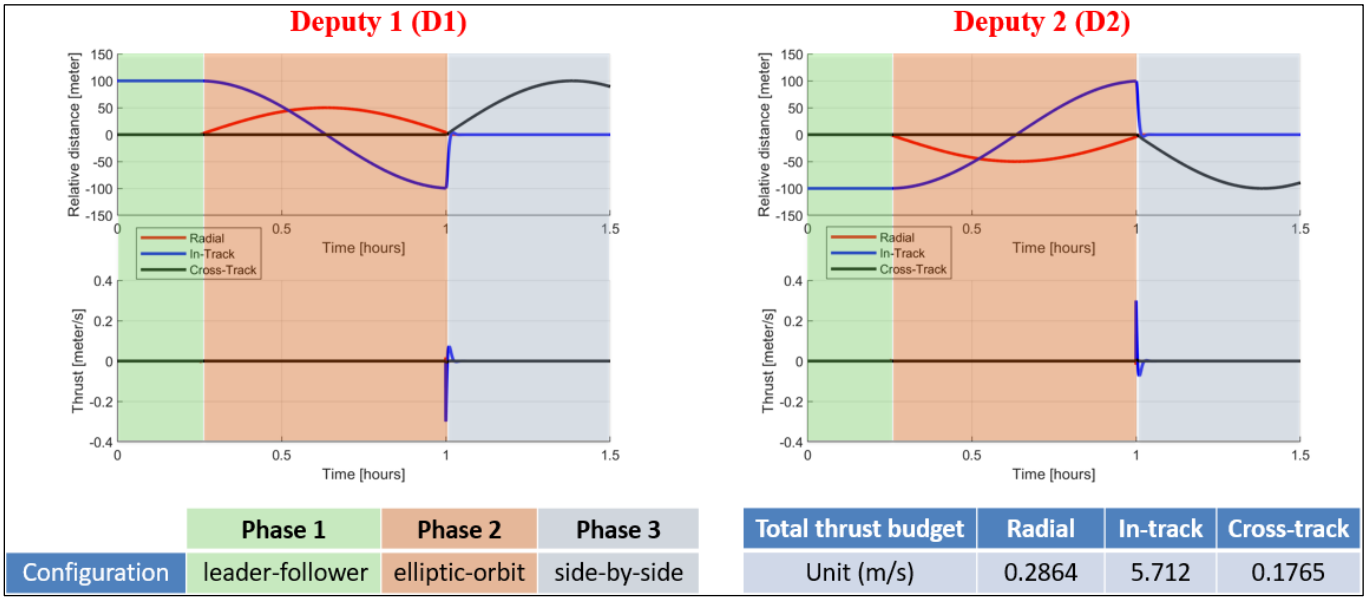

	Phase 1	Phase 2	Phase 3
Configuration	leader-follower	elliptic-orbit	side-by-side

Total thrust budget	Radial	In-track	Cross-track
Unit (m/s)	0.2864	5.712	0.1765

Fig. 7: Software simulation of the polar orbit formation flying scenario

RESULTS AND DISCUSSION

Applications of the three scenarios described in the previous section are now presented.

Multi-constellation Ionospheric Measurements in the Baseline ESF Scenario

The multi-constellation version of the VTFFTB was applied to simulate the baseline ESF scenario. GNSS data collected from a 1-hour simulation was processed using the ionospheric remote sensing system. GPS TEC was obtained using the L1 and L2 bands, and Galileo TEC was measured by E1 and E5b bands. The bias-free vertical TEC from the chief and deputy satellite for an individual PRN are used to retrieve the vertical N_e. Each vertical N_e is measured in between the two LEO receivers at a specific altitude. While the satellite fleet travels through different locations, a N_e profile projected vertically can be obtained by plotting N_e against central height (i.e. the altitude of middle point between the two satellites). Because the tracking duration is different between each PRN, a single PRN TEC typically can only cover a limited altitude range. So to obtain the vertical N_e retrieval profile across the full altitude range of the modelled (SR) N_e data, an averaging is performed on all the N_e measurements from a selected number of PRNs. Here, an outlier judgement process is applied to keep a selected number of PRNs that contribute their vertical N_e profiles to the averaging process. Finally, a low pass filter with a cutoff frequency of 0.01 Hz was applied to smooth the measurement results.

Compared to the GPS averaged N_e retrieval, using both GPS and Galileo to sense vertical N_e gives a more accurate retrieval result. As shown in Fig. 8 (a), the SR modelled N_e is plotted in red, the averaged filtered N_e from selected GPS and Galileo PRNs are plotted in black, and the measurement errors (difference between the model and the measurement) are plotted in green. In these results, the GNSS simulation was based on the almanac from July 13, 2018, when 13 Galileo satellites were operational. Compared to using GPS-only in this simulation, the absolute mean of N_e measurement errors was decreased by 32.83%. As the Galileo modernization progresses, more satellites have been launched. Another simulation of the baseline ESF scenario was done by using a more recent GNSS almanac from June 19, 2019, when 22 Galileo satellites were operational. The same processing routine was applied and the

vertical N_e retrieval result using both GPS and Galileo TEC are shown in Fig. 8 (b). This time, the absolute average error of N_e retrieval using both GPS and Galileo was further decreased to 37.79%, by comparing to the results when only using GPS selected PRNs. Therefore, further improvement of this N_e retrieval technique can be seen as the Galileo constellation grows.

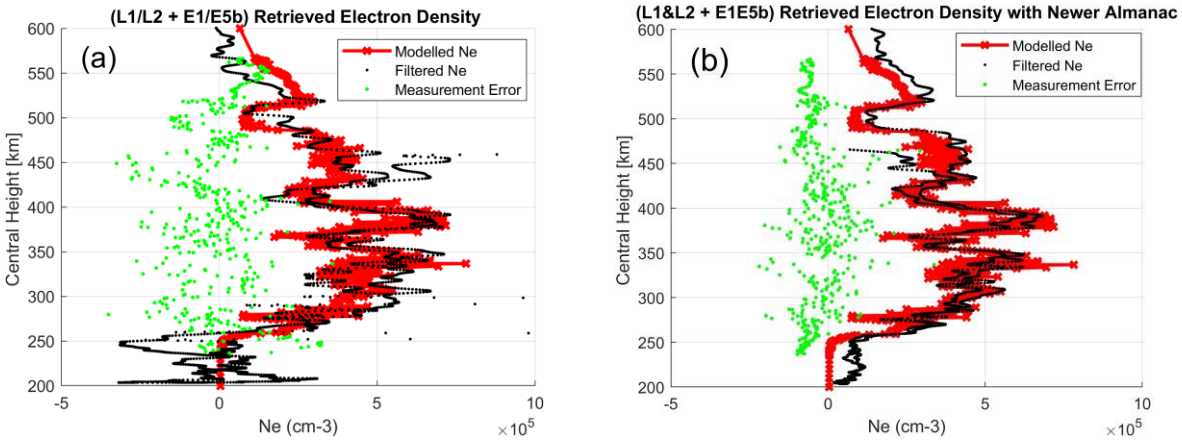

Fig. 8: N_e retrieval using both GPS and Galileo TEC: (a) July 13, 2018 almanac; (b) June 19, 2019 almanac

Besides TEC and vertical N_e, more space-based ionospheric scintillations can be observed by including the Galileo constellation. The signal frequency and power of GPS L1, L2, and L5, and Galileo E1, E5a, E5b and E5 AltBOC bands are different. According to the phase screen scintillation theory presented in [22], the size of ionospheric irregularities are associated with the GNSS signal wavelength. Therefore, scintillation observations from multiple frequencies are useful to identify the scales of ionospheric irregularities. As shown in Fig. 9 (a), the Galileo E1 S4 measured by the chief satellite (with a sampling rate of 20-Hz) from all 17 visible PRNs are plotted against the altitude. It is clear to see that the high level S4 events occurred within the cuboid plasma bubble region between 290 – 350 km. The same Galileo E1 S4 observations from the chief satellite system are plotted horizontally along its ground-track as shown in Fig. 9 (b). The region of high S4 events appeared, as expected, near the JRO region. The scintillation observations from the deputy satellite and other frequency bands are obtained as well. Incorporating the additional Galileo frequency bands increases the spatial coverage and provides more tomographic information for characterizing ionospheric structures [23].

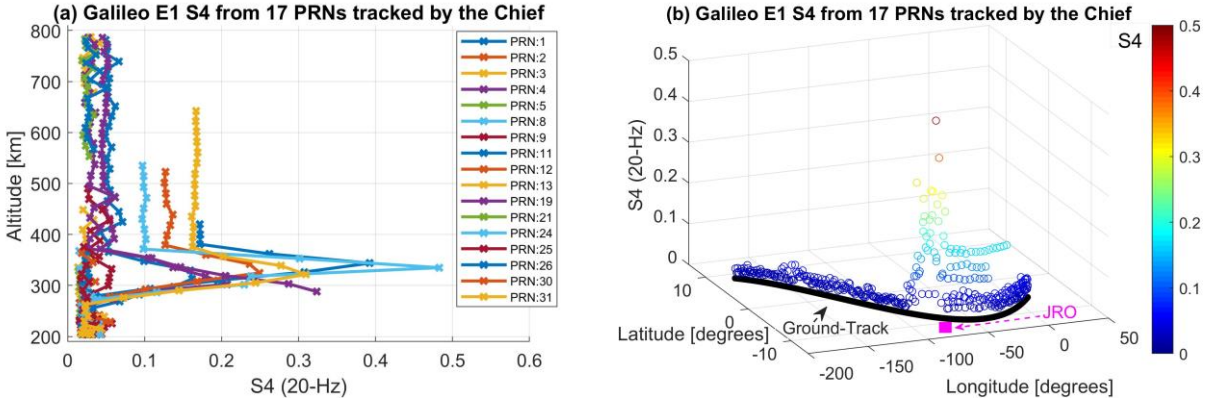

Fig. 9: Galileo E1 S4 observations by the chief satellite from a HIL simulation of June 19, 2019 almanac: (a) vertical view; (b) horizontal view

Multi-constellation N_e Retrieval using Natural Elliptic Relative Orbit Configurations in the ESF Scenario

Two configurations of natural (elliptic) orbits, demonstrated in Fig. 5 (a) & (b), are used to measure TEC and retrieve vertical N_e in the ESF scenario. After a one-hour HIL simulation with the OEM729 receiver, the vertical GPS (L1/L2) and Galileo (E1/E5b) TEC

measured from each visible PRN are processed to generate vertical N_e profiles. For GPS vertical N_e retrievals, the results from PRN No. 9 were selected due to the longest tracking duration, which covers the longest range of altitude coverage compared with other GPS PRN results. As shown in Fig. 10 (a), the vertical N_e measurements using the 2-km max radial offset configuration are plotted in blue against central height. The reference SR model N_e are plotted in red, while the measurement errors are computed and plotted in black. A second x-axis on top is introduced to visualize the height difference between the chief and deputy satellites (plotted in green) at each central height due to the natural elliptic motion. The average absolute error and standard deviation of errors are 1.2963×10^5 cm^{-3} and 3.7006×10^5 cm^{-3}, respectively. The measurement noise level not only depends on the particular receiver model and frequency band combination but also is sensitive to the height separation. The errors get larger when the height separation is small (e.g. less than ~500 meters). As a comparison, the vertical N_e measurements from the same PRN using the 10-km max radial offset configuration are plotted in Fig. 10 (b). Here, the average absolute error and standard deviation of errors are 7.1056×10^4 cm^{-3} and 2.5909×10^5 cm^{-3}, respectively. Since the height separation is larger for a larger period of time during the simulation , the measurements and measurement errors fluctuate less for the 10-km maximum separation elliptic orbit scenario compared to the 2-km maximum separation elliptic orbit scenario. For this particular SR N_e profile, the 10-km configuration achieves a more accurate overall measurement, however the N_e retrieval begins losing resolution when the height separation gets too large. For example, below the altitude of 400 km, the height difference becomes larger than 52 km and the vertical N_e measurements deviate more from the reference SR N_e model.

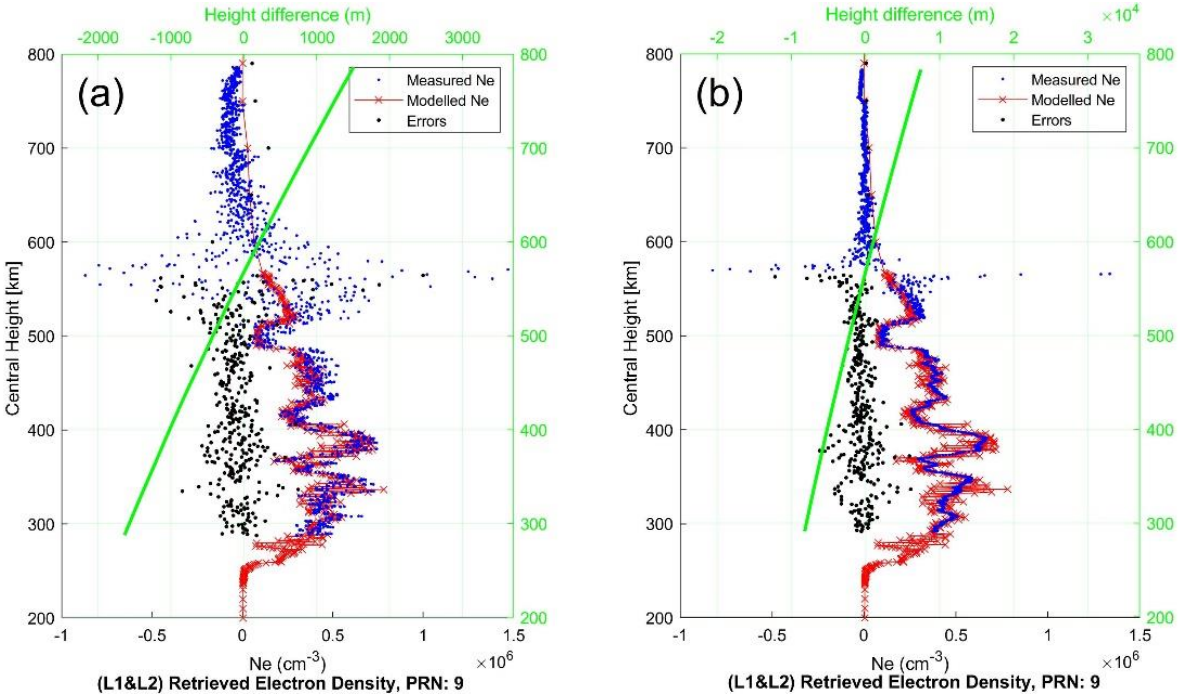

Fig. 10: N_e retrieval with GPS PRN 9 (L1/L2) TEC using elliptic orbit: (a) 2-km max radial offset; (b) 10-km max radial offset. Green line shows the variation of separation during the orbit. Note increase in error for small separation.

For Galileo N_e retrieval, PRN 4 results were selected due to a relative long tracking duration and altitude coverage (between ~ 220 km and ~ 483 km). The vertical N_e measurements using the 2-km max radial offset configuration are plotted in Fig. 11 (a), while the 10-km max radial offset configuration results are presented in Fig. 11 (b) for comparison. The average absolute error and standard deviation of errors in Fig. 11 (a) are 1.4710×10^5 cm^{-3} and 1.4284×10^5 cm^{-3}, respectively. Due to a nosier Galileo E1&E5b carrier-phase TEC, the associated Galileo vertical N_e is nosier in comparison to the GPS results in Fig. 10 (a). The smaller the height separation is, the more the N_e measurements fluctuate. The average absolute error and standard deviation of errors for the in Fig. 11 (b) are 5.3386×10^4 cm^{-3} and 1.0097×10^5 cm^{-3}, respectively. The 10-km radial offset measurements are less nosier than the 2-km's results. Therefore, a larger height separation formation configuration may be more appropriate for the Galileo TEC and N_e measurements with the OEM729 receiver in this scenario. The results discussed in this subsection demonstrate that the VTFFTB can be used to optimize formation configurations given a specific GNSS receiver.

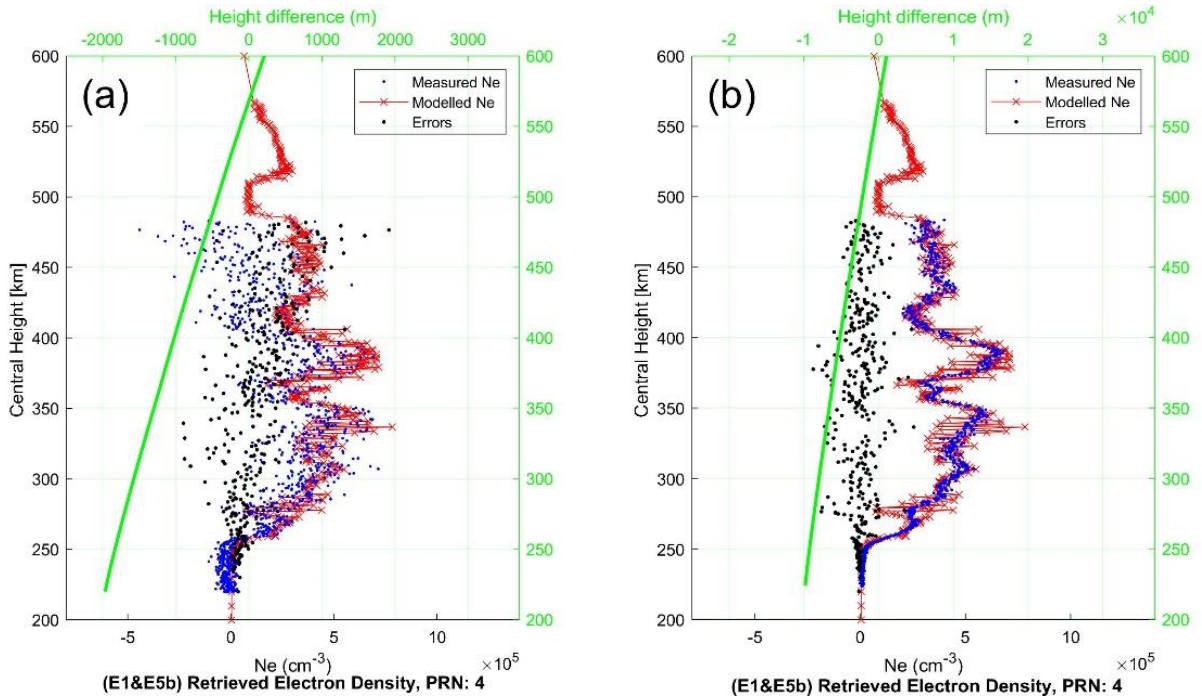

Fig. 11: N_e retrieval with Galileo PRN 4 (E1/E5b) TEC using elliptic orbit: (a) 2-km max radial offset; (b) 10-km max radial offset. Green line shows the variation of separation during the orbit. Note increase in error for small separation.

Real-time HIL Simulation of 3-satelllite Formation Flying

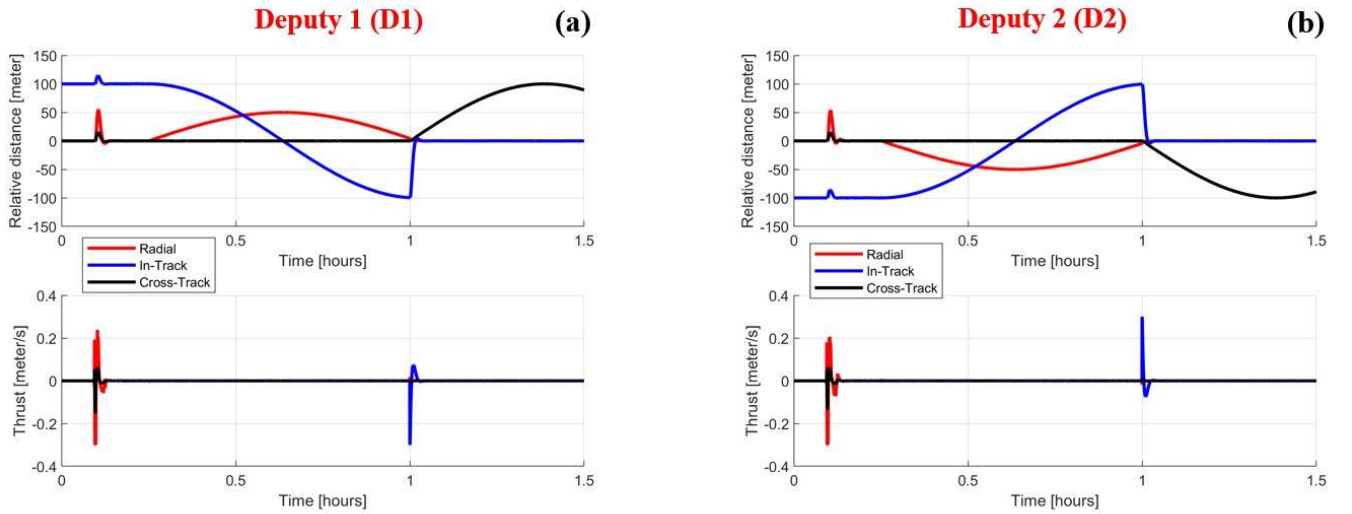

Total thrust budget	Radial	In-track	Cross-track
Unit (m/s)	10.99	8.836	3.559

Total thrust budget	Radial	In-track	Cross-track
Unit (m/s)	11.96	8.910	3.724

Fig. 12: HIL simulation results of the polar orbit formation flying scenario, including relative position history, thrust history, and total thrust. (a) Deputy 1 (b) Deputy 2

The 3-satellite version of VTFFTB was applied to simulate the polar orbit scenario. The relative position and thrust history of D1 are shown in Fig 12 (a), and the relative position and thrust history of D2 are shown in Fig 12 (b). Overall, the HIL simulation results are consistent with the software simulation results shown in Fig. 7, except an early moment of orbit deviation (indicated by the two green circles in the upper panels) happens during the phase I leader-follower formation. That is caused by relatively poor initial estimations when the first available estimation data is coming from the chief. As a result, the flight controller applied unnecessary thrust to deviate the two deputy satellites, which is observed as the transient near 0.1 hrs. A way to resolve this problem is to allow some time for the filter to initialize or further tune the EKF. Due to the deviation and other real time hardware simulation effects, the thrust consumed by both deputy are larger than the budget but still acceptable. This demonstrates the 3-satellite fleet real time formation flying simulation has been successfully working on the new VTFFTB.

SUMMARY AND CONCLUSIONS

The previous GPS-based VTFFTB has been successfully extended to a multi-constellation GNSS version with the addition of Galileo, and then applied to simulate an ESF (ionospheric plasma bubble) measurement scenario using two LEO formation flying satellites. HIL simulation shows the multi-constellation formation flying of GNSS receivers can achieve better accuracy when retrieving vertical N_e from differential TEC. Ionospheric scintillations can be observed through multiple frequency bands from a new constellation with a different modulation scheme. Two new formation configurations using natural elliptic orbit are simulated to offer a better fuel budget while measuring the vertical N_e with two GNSS receivers at different altitudes. Different characteristics of N_e retrieval are evaluated between different GNSS constellation using a specific GNSS receiver, which is beneficial for the optimal formation configuration design. By incorporating additional GNSS simulators and GNSS receivers for LEO navigation, a 3-satellite version of VTFFTB has been developed to simulate real-time HIL 3 spacecraft formation flying. A polar orbit scenario was designed and used to validate the real time simulation capability by running three-satellites on the VTFFTB. Three phases of formation configuration ("leader-follower", "elliptic", and "side-by-side") were used to test the maneuverability for future space weather measurement scenarios. Compared to single or two satellite formation flying, 3-satellite fleet is more advantageous study multi-scale ionospheric irregularities.

Future improvements of the VTFFTB infrastructure include further fine tuning of the EKF, more robust carrier-phase ambiguity estimation algorithm to address possible cycle clips scenarios, and more robust time synchronization. This will enhance the robustness of GNSS differential measurement model in the navigation & control system. The new 3-satellite version of the VTFFTB has been validated. Further studies will be done to investigate new space weather applications using TEC, derived N_e and scintillation measurements. A new method to integrate a software-based ionosphere model (e.g. 3D N_e profile with temporal variation) and the RF GNSS signals output from the simulator is currently under investigation in order to more accurately model ionospheric structures. These results of this work will be reported on in the near future.

ACKNOWLEDGMENTS

The authors would like to thank Gregory D. Earle and Anthea J. Coster for providing useful suggestions. The VTFFTB was supported by the AFOSR (grant 13-0658-09) and Virginia Tech. Michael Hartinger was supported by NSF grants PLR-1744828 and PLR-1543364.

REFERENCES

[1] Komjathy, A., Galvan, D. A., Stephens, P., Butala, M. D., Akopian, V., Wilson, B., Verkhoglyadova, O., Mannucci, A. J. and Hickey, M., "Detecting ionospheric TEC perturbations caused by natural hazards using a global network of GPS receivers: The Tohoku case study", *Earth, planets and space*, *64*(12), 2012, pp. 1287-1294.

[2] Curtis, S., "The magnetospheric multiscale mission... resolving fundamental processes in space plasmas", Technical Report, 1999.

[3] Escoubet, C. P., Schmidt, R. and Goldstein, M. L., "Cluster-Science and mission overview", *The Cluster and Phoenix Missions*, Springer, Dordrecht, 1997, pp. 11-32.

[4] Bandyopadhyay, S., Foust, R., Subramanian, G. P., Chung, S. J. and Hadaegh, F. Y., "Review of formation flying and constellation missions using nanosatellites", Journal of Spacecraft and Rockets, (0), 2016, pp. 567-578.

[5] Kintner, P. M. and Ledvina, B. M., "The ionosphere, radio navigation, and global navigation satellite systems", *Advances in Space Research*, *35*(5), 2005, pp.788-811.

[6] Vierinen, J., Coster, A. J., Rideout, W. C., Erickson, P. J., and Norberg, J., "Statistical framework for estimating GNSS bias", *Atmos. Meas. Tech.*, 9, 2016, pp. 1303-1312.

[7] Jin, S., Cardellach, E., and Xie, F., GNSS Remote Sensing Theory, Methods and Applications, Springer, 2014, pp. 79-90.

[8] Anthes, R. A., Ector, D., Hunt, D. C., Kuo, Y. H., Rocken, C., Schreiner, W. S., Sokolovskiy, S. V., Syndergaard, S., Wee, T. K., Zeng, Z. and Bernhardt, P. A., "The COSMIC/FORMOSAT-3 mission: Early results", Bulletin of the American Meteorological Society, 89(3), 2008, pp. 313-333.

[9] Irisov, V., Nguyen, V., Duly, T., Masters, D. S., Nogues-Correig, O., Tan, L., Yuasa, T. and Ector, D. R., "Recent Ionosphere Collection Results From Spire's 3U CubeSat GNSS-RO Constellation", In *AGU Fall Meeting* Abstracts, 2018.

[10] Gentile, L. C., Burke, W. J. and Rich, F. J., "A climatology of equatorial plasma bubbles from DMSP 1989–2004", *Radio Science*, 41(5), 2006.

[11] Yizengaw, E., Moldwin, M. B., Dyson, P. L. and Essex, E. A., "Using tomography of GPS TEC to routinely determine ionospheric average electron density profiles", *Journal of Atmospheric and Solar-Terrestrial Physics*, 69(3), 2007, pp. 314-321.

[12] Peng, Y., Scales, W., and Edwards, T. R., "GPS-based Spacecraft Formation Flying Simulation and Applications to Ionospheric Remote Sensing", *Proceedings of the 31st International Technical Meeting of the Satellite Division of The Institute of Navigation (ION GNSS+ 2018)*, Miami, Florida, USA, 2018, pp. 2518–2534.

[13] Peng, Y. and Scales, W., "Satellite Formation Flight Simulation Using Multi-constellation GNSS and Applications to Ionospheric Remote Sensing", In *AGU Fall Meeting* Abstracts, 2018.

[14] Busse, F. D., How, J. P. and Simpson, J., "Demonstration of adaptive extended Kalman filter for low earth orbit formation estimation using CDGPS", *Navigation*, 50(2), 2003, pp. 79–93.

[15] Cloutier, J. R., "State-dependent Riccati equation techniques: an overview", *American Control Conference*, IEEE, vol. 2, 1997, pp. 923–936.

[16] Park, J. I., Park, H. E., Park, S. Y. and Choi, K. H., "Hardware-in-the-loop simulations of GPS-based navigation and control for satellite formation flying", *Advances in Space Research*, Vol. 46, No. 11, 2010, pp. 1451–1465.

[17] Rodrigues, F. S., Hickey, D. A., Zhan, W., Martinis, C. R., Fejer, B. G., Milla, M. A. and Arratia, J. F., "Multi-instrumented observations of the equatorial F-region during June solstice: large-scale wave structures and spread-F", *Progress in Earth and Planetary Science*, *5*(1), 2018, p. 14.

[18] Rino, C. L., Tsunoda, R. T., Petriceks, J., Livingston, R. C., Kelley, M. C. and Baker, K. D., "Simultaneous rocket-borne beacon and in situ measurements of equatorial spread F—Intermediate wavelength results". *Journal of Geophysical Research: Space Physics*, 86(A4), 1981, pp. 2411-2420.

[19] Wiesel, W. E., "*Spaceflight dynamics*", Third Edition, CreateSpace, 2010, pp. 86-90.

[20] Clauer, C. R., Kim, H., Deshpande, K., Xu, Z., Weimer, D., Musko, S., Crowley, G., Fish, C., Nealy, R., Humphreys, T. E. and Bhatti, J. A., "An autonomous adaptive low-power instrument platform (AAL-PIP) for remote high-latitude geospace data collection", *Geoscientific Instrumentation, Methods and Data Systems*, *3*(2), 2014, pp. 211-227.

[21] Greenwald, R. A., Baker, K. B., Dudeney, J. R., Pinnock, M., Jones, T. B., Thomas, E. C., Villain, J. P., Cerisier, J. C., Senior, C., Hanuise, C. and Hunsucker, R. D., "Darn/superdarn", *Space Science Reviews*, *71*(1-4), 1995, pp. 761-796.

[22] Yeh, K. C. and Liu, C. H., "Radio wave scintillations in the ionosphere", *Proceedings of the IEEE*, *70*(4), 1982, pp.324-360.

[23] Morton, Y., Bourne, H., Carroll, M., Jiao, Y., Kassabian, N., Taylor, S., Wang, J., Xu, D. and Yin, H., " Multi-constellation GNSS observations of equatorial ionospheric scintillation", *Proceedings of the 2014 XXXIth URSI General Assembly and Scientific Symposium (URSI GASS)*, IEEE, 2014, pp. 1-4.